University of Groningen

Dynamic poly(disulfide)s for sustainable materials

Deng, Yuanxin

DOI:
10.33612/diss.208714129

IMPORTANT NOTE: You are advised to consult the publisher's version (publisher's PDF) if you wish to cite from it. Please check the document version below.

Document Version
Publisher's PDF, also known as Version of record

Publication date:
2022

Link to publication in University of Groningen/UMCG research database

Citation for published version (APA):
Deng, Y. (2022). *Dynamic poly(disulfide)s for sustainable materials*. University of Groningen.
https://doi.org/10.33612/diss.208714129

Copyright
Other than for strictly personal use, it is not permitted to download or to forward/distribute the text or part of it without the consent of the author(s) and/or copyright holder(s), unless the work is under an open content license (like Creative Commons).

The publication may also be distributed here under the terms of Article 25fa of the Dutch Copyright Act, indicated by the "Taverne" license. More information can be found on the University of Groningen website: https://www.rug.nl/library/open-access/self-archiving-pure/taverne-amendment.

Take-down policy
If you believe that this document breaches copyright please contact us providing details, and we will remove access to the work immediately and investigate your claim.

Downloaded from the University of Groningen/UMCG research database (Pure): http://www.rug.nl/research/portal. For technical reasons the number of authors shown on this cover page is limited to 10 maximum.

Download date: 04-06-2022

Chapter 2

Toughening a Self-healable Supramolecular Polymer by Ionic Cluster-enhanced Iron-Carboxylate Complexes

Published as:

Angew. Chem. Int. Ed. **2020**, 59, 5278-5283

Yuanxin Deng, Qi Zhang, Ben L. Feringa*, He Tian, and Da-Hui Qu*

Abstract:

Supramolecular polymers that can heal themselves automatically usually exhibit weakness in mechanical toughness and stretchability. Here we exploit a toughening strategy for a dynamic dry supramolecular network by introducing ionic cluster-enhanced iron-carboxylate complexes. The resulting dry supramolecular network simultaneous exhibits tough mechanical strength, high stretchability, self-healing ability, and processability at room temperature. The high performance of these distinct supramolecular polymers is attributed to the hierarchical existence of four types of dynamic combinations in the high-density dry network, including dynamic covalent disulfide bonds, noncovalent H-bonds, iron-carboxylate complexes and ionic clustering interactions. The extremely facile preparation method of this self-healing polymer offers prospects for high-performance low-cost material among others for coatings and wearable devices.

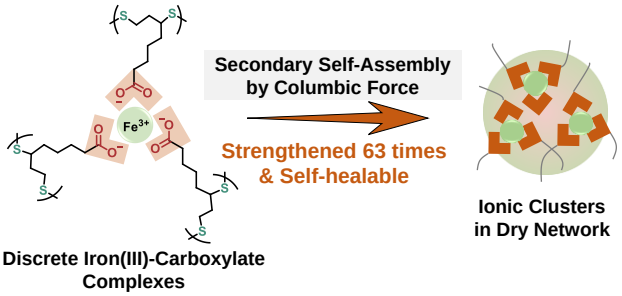

2.1 Introduction

Polymers that undergo autonomous healing are mimicking intrinsic properties of biosystems and are highly desirable for many applications because they can endow materials with the capability to repair mechanical damage.[1] To realize self-healing properties, some strategies have been developed, especially using dynamic reversible noncovalent transformations to induce the reformation of damaged interfaces.[2-7] Taking advantage of the supramolecular toolbox i.e. H-bonds,[2] host-guest combinations,[3] metal-ligand interactions,[4] ionic bonds,[5] dynamic covalent bonds,[6] dipole-dipole interactions,[7] and even van der Waals force,[1e] have shown to be versatile features in the design of self-healing gels and polymers. However, there remain some very challenging issues facing the design of a self-healing supramolecular network: i) The introduction of weak but reversible noncovalent bonds into the network usually decreases significantly the stiffness of the network, leading to a self-healing but soft network; ii) The introduction of noncovalent bonds, especially based on hierarchical multi-component systems often requires complex synthetic procedures increasing material costs; iii) Many self-healing polymers contain or involve external solvents to support the supramolecular recognition processes, while developing self-healable dry polymers is more preferable for industrial application.[1, 2, 8]

Very recently, our lab developed an unprecedented supramolecular polymer using the natural small molecule,[8] thioctic acid (TA), as the main feedstock. A crosslinked solid polymer was obtained by a facile co-mixing method of molten TA liquid, 1,3-diisopropenylbenzene (DIB) and minimal $FeCl_3$, involving no external solvent. The crosslinked supramolecular network is capable to function as a self-healable elastomer at ambient temperatures. However, the resulting materials exhibit very low mechanical moduli of less than 90 kPa, limiting further applications in high-strength self-healable materials. The weakness in mechanical moduli mainly rested on the discrete distribution of iron-carboxylate complexes and demanded for a toughening strategy applicable to a dynamic self-healing system. We anticipated that the secondary clustering interactions of these ionic complexes could possibly strengthen the dynamic supramolecular network by high-affinity Coulombic force, especially to be expected in a solvent-free dry network.

2.2 Results and Discussion

2.2.1 Molecular design and synthesis

We demonstrate that a dry supramolecular network can be remarkably toughened by abundant iron-ion crosslinking (1% molar ratio of monomer TA) (Fig. 2.1), enhancing the mechanical moduli of the polymers over 60 times, meanwhile maintaining the high stretchability and self-healing capability of the dynamic network. The ionic cluster effect of iron-carboxylate complexes is found to be a secondary crosslinking interaction in this solvent-free network. Significantly, three commercial feedstocks and a little heat are all that's needed to make such high-performance supramolecular polymers that simultaneously integrate high toughness, high stretchability, self-healing ability, processability, and recyclability. We envision that this developed dynamic network offers opportunities towards applications in low-cost high-performance self-healing materials.

The preparation of poly(TA-DIB-Fe) copolymers with high iron(III)-to-TA molar ratio (1/1000 to 1/50) was based on a modification of our previous procedure[8]. Specifically, a higher heating temperature (150°C) was used to decrease the viscosity of the liquid mixture, and the reaction mixture was sealed to protect the system from humidity in air in view of the hydrophilic nature of abundant iron-carboxylate ionic clusters (Experimental section and Fig. S1). Upon cooling the molten mixture of TA, DIB, and $FeCl_3$ to room temperature yellow to brown polymer solids are obtained. Increasing the iron(III) concentration, the sample with an iron(III)-to-TA molar ratio (1/100) turned brown, revealing the formation of ionic clusters due to the typical ligand-to-metal charge transfer.[9] The polymer film exhibited translucency (Fig. 2.2), which indicated the homogeneous nature of the resulting network.

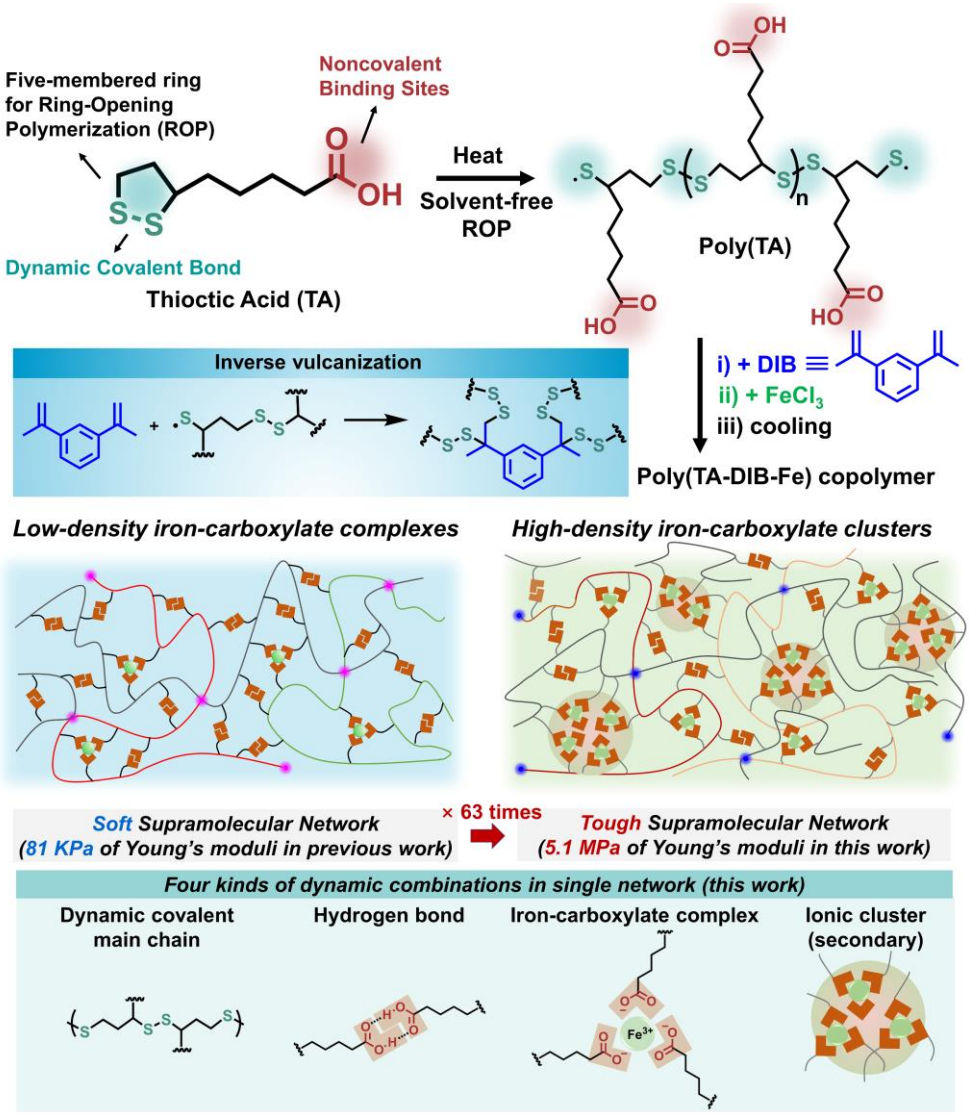

Figure 2.1 Schematic representation of the TA monomer and poly(TA) polymers. The cartoon representation shows the existed four types of dynamic combinations in the network.

2.2.2 Characterization of structure

To further investigate the high-density iron-carboxylate clusters in the material, X-ray diffraction (XRD) was performed, showing the absence of iron oxide species. The observed broad peaks at around 20° indicated the amorphous nature of the poly(TA-DIB-Fe) copolymer network with the iron(III)-to-TA molar ratio lower than 1/500 (Fig. 2.2A) in accordance with our previous study[8]. However, notable sharp diffraction peaks at 21.2° and 23.6° were observed in the sample with an iron(III)-to-TA molar ratio of 1/100 and 1/50 (Fig. 2.2A), pointing to the formation of metal ionic clusters by Coulombic force among the iron-carboxylate complexes.[10]

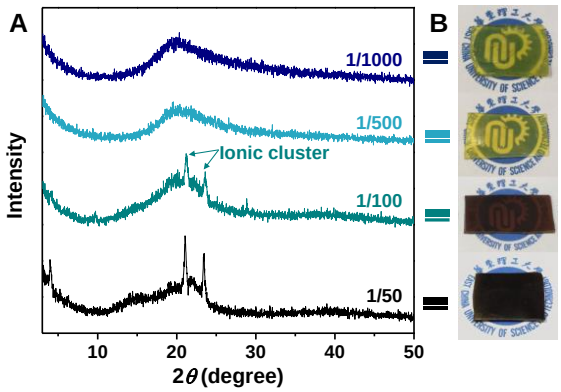

Figure 2.2 XRD patterns (A) and photographs (B) of the poly(TA-DIB-Fe) films [iron(III)-to-TA molar ratio of 1/1000, 1/500, 1/100, and 1/50].

Recent literature shows that ionic cluster formation of iron(III)-ligand complexes in a dry polymer network can result in nanosized internal order.[11] To get further information of the ionic clusters, synchrotron radiation small-angle X-ray scattering (SAXS) was employed (Fig. 2.3). As a result, all of the poly(TA-DIB-Fe) samples showed no sharp peaks at the tested region, indicating the disordered distribution of the iron-carboxylate clusters in the network. Moreover, grazing-incidence wide-angle X-ray scattering (GIWAXS) further confirmed the amorphous nature of the network by the absence of scattering signals at wide angles (Fig. 2.4). Therefore, the high-density iron(III)-carboxylate complexes in the dry network existed as disordered ionic clusters.

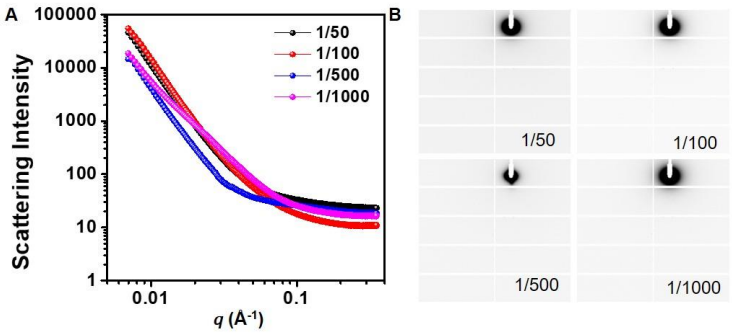

Figure 2.3 (A) Synchrotron radiation small-angle X-ray scattering (SAXS) spectrum of the poly(TA-DIB-Fe) copolymer [iron(III)-to-TA molar ratio of 1/1000, 1/500, 1/100, and 1/50]. (B) 2D SAXS patterns of the poly(TA-DIB-Fe) copolymers.

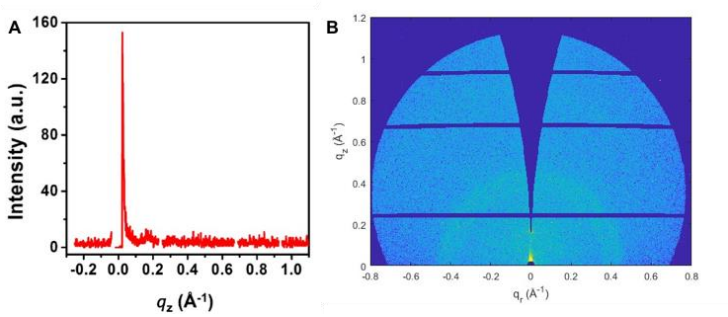

Figure 2.4 Grazing-incidence wide-angle X-ray scattering (GIWAXS) spectrum of the poly(TA-DIB-Fe) copolymer [iron(III)-to-TA molar ratio of 1/100]. (A) 1D spectrum; (B) 2D pattern.

Polymer materials containing ionic bonds usually exhibit humidity-responsive properties.[12] The water in the air could enter into the network and hydrate the ionic bonds, resulting in the remarkable decrease in mechanical strength,[12a] which might become a disadvantage in practical applications. Surprisingly, the poly(TA-DIB-Fe) copolymers crosslinked by high-density ionic clusters exhibited excellent humidity-resistance ability, while a reference sample without DIB would be gradually softened and become out-of-shape in the air (Fig. 2.5A). The disappearance of ionic cluster signals in the XRD patterns also indicated the hydration-induced dissociation of the iron(III)-carboxylate ionic clusters in the poly(TA-Fe) network (Fig. 2.5B). The infrared spectra indicated a low content of hydrated water in the DIB-crosslinked network (Fig. 2.5C).

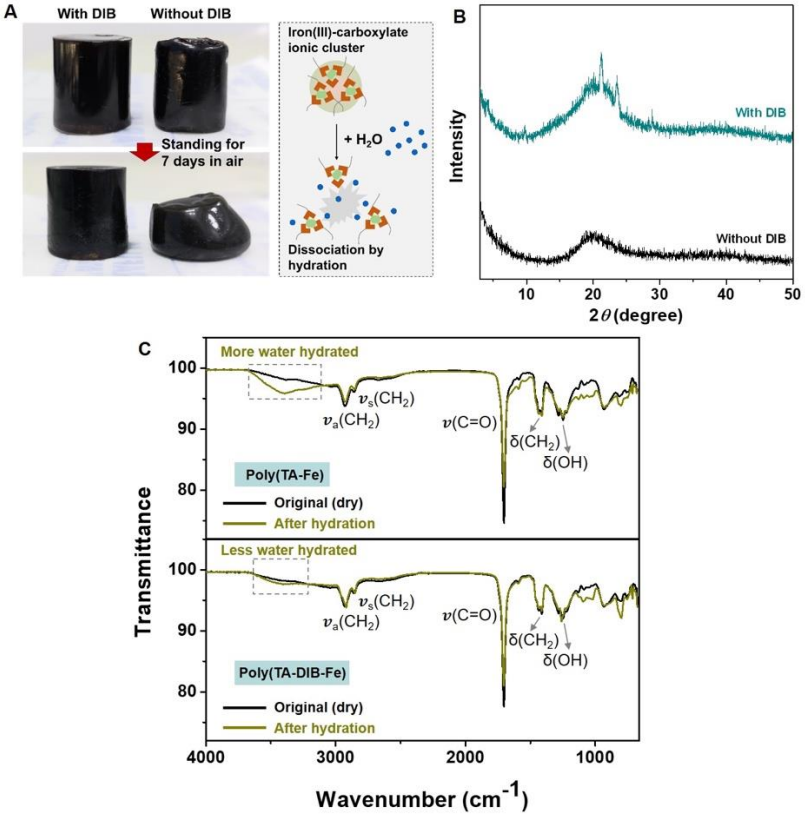

Figure 2.5 (A) Photographs showing the different humidity-resistance of the poly(TA-DIB-Fe) and poly(TA-Fe) polymer. Two cylindrical polymer samples are placed in air condition. After standing for 7 d, the sample with DIB shows the original shape, while the other without DIB is out of the original shape due to humidity-induced softening. (B) XRD patterns of the poly(TA-DIB-Fe) and hydrated poly(TA-Fe) polymers. The disappearance of the ionic peaks in the sample without DIB indicated the hydration-induced dissociation of the high-density iron(III)-carboxylate ionic clusters in the network. (C) ATR-FTIR spectra of the poly(TA-Fe) copolymer (top) and poly(TA-DIB-Fe) copolymer (bottom) before and after hydration. The iron(III)-to-TA molar ratio of all the samples is 1/100. There was no signal of HCl (2886 cm^{-1}) detected in the FT-IR spectra of the polymer, indicating the absence of HCl in the network.

Compared to poly(TA-Fe), poly(TAH-DIB-Fe) showed higher stiffness and maximal tensile stress owing to the existence of DIB-crosslinks and ionic clusters (Fig. 2.6). Moreover, the ionic-cluster-toughened network was more stable to humidity and insoluble in water in the presence of DIB (Fig. 2.6 and S2), which should be attributed to the shielding effect of the highly hydrophobic DIB units. Unexpectedly, slight enhanced mechanical strength after hydration was observed for DIB-crosslinked network after hydration. This might be attributed to the presence of partial phase separation in the network after hydration, which can be beneficial for the noncovalent sacrificial bond mechanism.

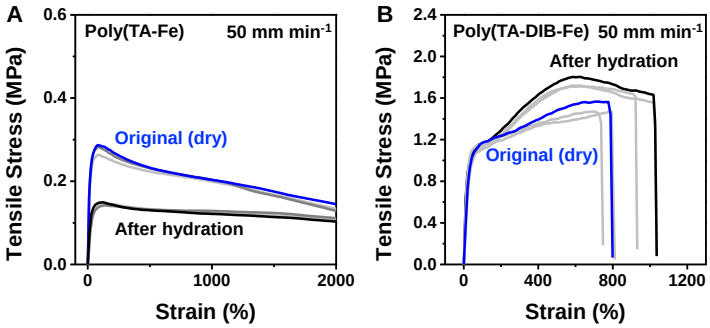

Figure 2.6 Stress-strain curves of the (A) poly(TA-Fe) copolymer and (B) poly(TA-DIB-Fe) copolymer before and after hydration. The iron(III)-to-TA molar ratio of all the samples is 1/100. The strain speed is 50 mm min^{-1}.

Broadband dielectric spectroscopy (BDS) of the resulting poly(TA-DIB-Fe) copolymers with varied iron(III)-to-TA molar ratios (1/50, 1/100, 1/500, 1/1000) revealed the consistent frequency-dependent conductivity and surface resistance expected for insulator materials (Fig. S3).[13] The variation of the amount of iron(III) ions resulted in slight differences of the dielectric properties of the poly(TA-DIB-Fe) copolymers. However, the hydration of the poly(TA-Fe) sample without DIB led to the remarkable increases in dielectric constant, dielectric loss, and conductivity (Fig. S3), which was attributed to the absorbed water molecules and enhanced mobility of the polymer chains.[14]

2.2.3 Mechanical properties

Combining the observed results of XRD, SAXS, GIWAXS, and BDS, it can be concluded that the high-density iron(III)-carboxylate complexes existed as ionic

clusters in the dry network of poly(TA-DIB-Fe) copolymer. This observation led us to the further exploration of how these ionic clusters affected the mechanical properties of the poly(TA-DIB-Fe) copolymers. The temperature sweeping rheological curves indicated enhanced mobility of the polymer chain with increasing temperature, supporting the noncovalently crosslinked nature of the network (Fig. 2.7).

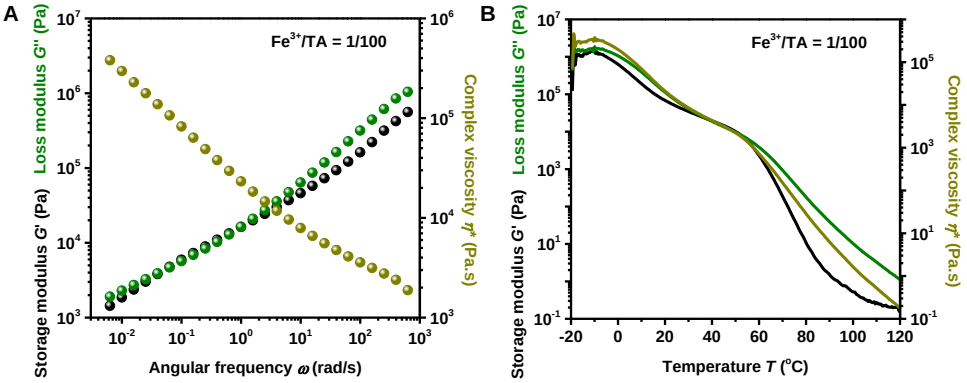

Figure 2.7 Rheology experiments of the poly(TA-DIB-Fe) copolymer with an iron(III)-to-TA molar ratio of 1/100. Frequency-dependence at 25°C (A) and temperature-dependence at 1 Hz (B) of storage (G'), loss (G'') moduli, and viscosity (η) are shown.

With the increasing iron(III)-to-TA molar ratio's ranging from 1/18000 to 1/50, the maximal tension strength increased from 0.05 MPa to 1.87 MPa, while the Young's modulus increased from 0.086 ± 0.01 MPa to 7.78 ± 0.46 MPa (Fig. 2.8A and Table S1). This large enhancement showed the remarkably toughened mechanical performance of the network after crosslinking by high-density iron(III)-carboxylate clusters. The toughening mechanism was attributed to the secondary high-affinity ionic bonding of the iron(III)-carboxylate complexes (Fig. 2.8B).[12a, 15] The toughened poly(TA-DIB-Fe) network with an iron(III)-to-TA molar ratio of 1/100 exhibited typical rate-dependent tensile curves (Fig. 2.8C), in which the sample can be stretched to over 6500% of its original length (Fig. 2.8D) at a lower strain rate of 20 mm min^{-1}. The stretched sample could be also recovered partially (Fig. S4). The high stretchability of the toughened polymer might be attributed to the hierarchical operation of four types of dynamic combinations which work as sacrificial bonds upon stretching (Fig. 2.8B).

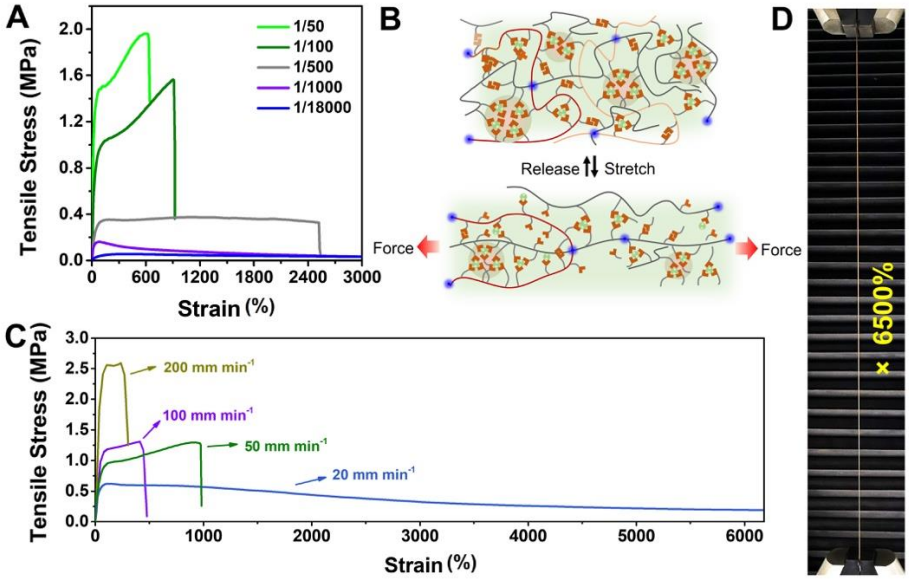

Figure 2.8 (A) Stress-strain curves of the copolymer with different iron(III) concentrations at a loading rate of 50 mm min^{-1} [Iron(III)-to-TA molar ratio of 1/50, 1/100, 1/500, 1/1000 and 1/18000, respectively]. (B) Energy dissipation mechanism for high toughness and stretchability. (C) Stress-strain curves of the copolymer at varied strain rates. (D) Photograph of the stretched polymer with an elongation of 6500%.

The resulting poly(TA-DIB-Fe) network with an iron(III)-to-TA molar ratio of 1/100 also showed good elasticity. The sample can undergo a complex tension-relaxation process without breaking despite the absence of resting time (Fig. 2.9A). The cyclic experiments also showed the successful recovery of elastic modulus and high Young's modulus with 5 min test intervals (Fig. 2.9B). A shorter resting time of 10 s leads to an incomplete recovery of the stretched polymer (Fig. S5). These results suggest a sliding mechanism based on dynamic chemical bonds, which required time to realize the strain recovery. Different from the soft poly(TA-DIB-Fe) copolymer crosslinked by low-density iron(III)-carboxylate complexes,[8] the ionic-cluster-toughening poly(TA-DIB-Fe) copolymer exhibited strikingly increased stress-affordability. The creep experiments indicated that only 20% strain was induced after a load of 57.2 kPa for 1 h (Fig. S6), while the copolymer with iron(III)-to-TA molar

ratio of 1/18000 can only sustain a load of 17.4 kPa for 400 s with a strain over 500%.[8] Moreover, a cylindrical copolymer can sustain a load of 2 kg, and a copolymer film with a thickness of 2 mm can lift a weight of 4.1 kg (Fig. S7). These results indicated the remarkable toughened network of the poly(TA-DIB-Fe) copolymer enforced by the ionic cluster formation.

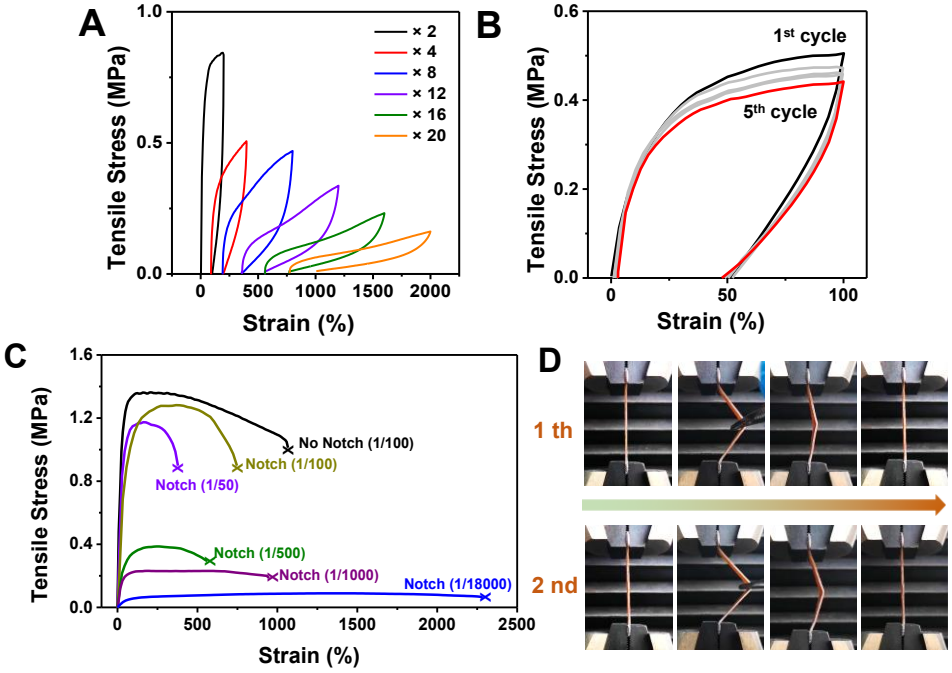

Figure 2.9 (A) Sequential loading-unloading stress-strain curves with no resting internals at a loading rate of 50 mm min^{-1}. (B) Five loading-unloading cycles of the copolymer with 5 min rest intervals at a loading rate of 20 mm min^{-1}. (C) Stress-strain curves of the 1/2 notched copolymer films with varied iron contents at a loading rate of 50 mm min^{-1}. The tensile stress of the notched samples has been corrected by the real area after notching. (D) Photographs showing the excellent elasticity. Unless otherwise indicated, the iron(III)-to-TA molar ratio of tested samples was 1/100.

The toughness of the resulting polymer was further investigated by the stress-strain experiment of a notched copolymer film with a 1/2 width scar. The notch experiments were performed using the copolymer with varied iron contents (1/100, 1/500, 1/1000, 1/18000) at two kinds of strain speeds (20 mm min^{-1} and 50 mm min^{-1}). As a result,

all of the samples exhibited similar stretchability at a strain rate of 20 mm min^{-1} (Fig. S8). The higher strain rate would decrease the breaking elongation of the notch samples (Fig. 2.9C and S9), which supported the proposed energy dissipation mechanism by noncovalent bonds because this noncovalent dissipation process usually exhibits dependence on deformation rates.[2d] All the samples with varied iron(III) ion contents exhibited considerable anti-tearing ability (Fig. S10). For the poly(TA-DIB-Fe) copolymer with an iron(III)-to-TA molar ratio of 1/100, the sample with 1/2 notch can be stretched into over 700% at the strain rate of 50 mm min^{-1}, suggesting that this ionic-cluster-toughened strategy can maintain the anti-tearing ability of the network. Meanwhile, a pre-stretched (200%) copolymer film can be also stretched in the vertical direction (Fig. 2.9D), which can be self-recovered after release. This process can be repeated several times, showing its good elasticity.

2.2.4 Self-healing ability

High mechanical strength usually leads to low dynamics and as a consequence inhibits the self-healing capability of materials, which represents a wide trade-off in the design of self-healable materials.[1f, 2b, 4c, 16] Taking advantage of the interplay of four types of dynamic combinations (i.e. dynamic chemical bonds and non-covalent interactions) in the network, we next focused on studying the self-healing performance of the ionic-cluster-toughened poly(TA-DIB-Fe) copolymer with an iron(III)-to-TA molar ratio of 1/100. We observed that a) A scratch on the copolymer film can be basically repaired at room temperature in 24 h (Fig. 2.10A); b) A cylindrical sample can be healed automatically by contacting the cut interfaces. (Fig. S11); c) The healed sample exhibited high stretchability (Fig. 2.10B); d) The self-healing process can be also performed in water (Fig. 2.10C). To quantitatively evaluate the self-healing performance, the stress-strain curve of the healed sample at room temperature after 24 h was tested, showing an excellently recovered mechanical strength and stretchability (Fig. 2.10D, and S12). The self-healing efficiency also exhibited a typical time-dependent feature (Fig. S13). This efficient self-healing ability of the resulting copolymer should be attributed to the synergetic dynamic exchange process of the existing four types of dynamic combinations in the dry network, that is dynamic covalent disulfide bonds, hydrogen bonds, iron(III)-carboxylate complexes and ionic clusters.

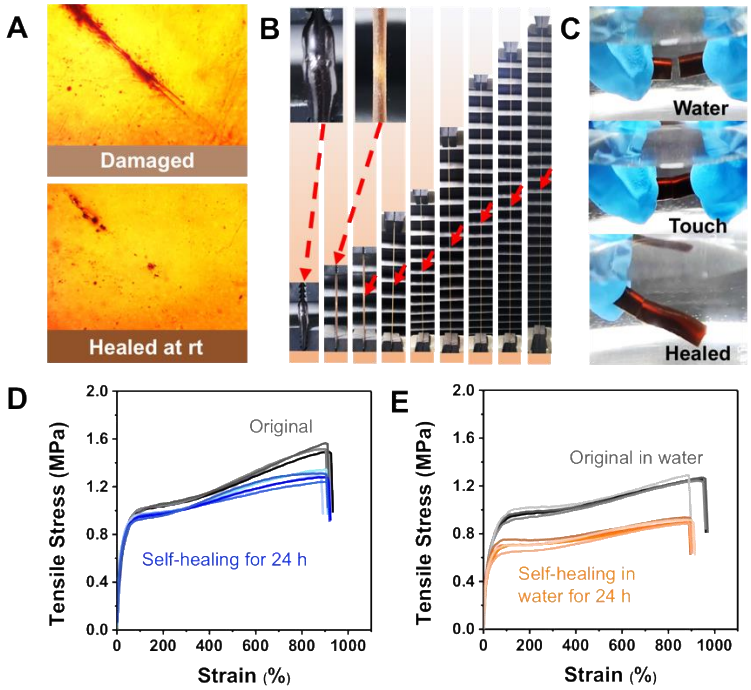

Figure 2.10 (A) Optical microscope images of the damaged and healed polymer showing the auto-restoration at room temperature for 24 h. (B) Optical images of poly(TA-DIB-Fe) at different strains with a loading rate of 20 mm min^{-1}. (C) Bisected the copolymer cylinder to two pieces and put together under water condition for self-healing. (D, E) Stress-strain curves of the original and healed samples of poly(TA-DIB-Fe) copolymer in air (D) and in water (E) for 24 h at room temperature. Parallel self-healing experiments were performed 5 times to show reproducibility. The iron(III)-to-TA molar ratio was 1/100. Tensile speed is 50 mm min^{-1}.

The self-healing ability is usually inhibited by the presence of water especially for H-bond-mediated repairing examples.[7, 16a] The quantitative self-healing experiments were performed in water, and the mechanical tensile test showed a good healing efficiency (Fig. 2.10E), in which the mechanical strength recovered 93.9% of the original moduli and the breaking elongation fully recovered. The good self-healing efficiency under water might be attributed to the presence of dynamic ionic bonds at the interfaces.[2f, 5] To evaluate the water-stability of the ionic-cluster-toughened network, soaking in water for several days led to no swelling or dissolution (Fig. S14).

Therefore, our copolymer materials simultaneously exhibited high mechanical toughness, high stretchability, and room-temperature self-healing capability. To compare this performance with previous reported materials (self-healing at room temperature),[1a,1e,2a,2d,2e,4a,4b,4d,8,5b,6e,7,17] we summarized the modulus (mechanical strength) and breaking elongation (stretchability) of the recently reported synthetic polymer materials that can undergo self-healing at room temperature (Fig. 2.11). The simultaneous realization of leading modulus and breaking elongation in single self-healing material system indicates the effectiveness of the ionic-cluster-toughening strategy in such a solvent-free and dynamic supramolecular network.

A

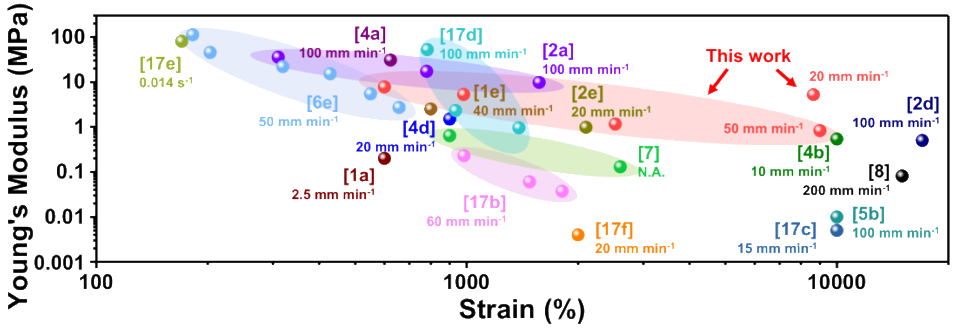

B

H-bonds	Van der Waals	Metal-ligand Coordination	Ionic Associations	Nitrogen Coordination Boroxines	Ion-Dipole	Covalent crosslinks
[1a], [2a], [2d], [8], [17e], [17d], [17b], [17c]	[1e]	[2e](Fe^{3+}), [4a](Zn^{2+}), [4b](Fe^{3+}), [4d](Eu^{3+}), [8](Fe^{3+})	[5b] [17c]	[6e]	[7]	[17e]

Figure 2.11 (A) Comparison of the present system to recent literature studies on self-healable elastomers at room temperature, which are marked with reference codes and strain rates in the diagram; (B) Design features for self-healable elastomers.

Polymers that can be reused in a mild and energy-saving process are of great importance due to rising environmental, materials recycling and energy issues.[18] The self-healing ability enabled an easy processability of the poly(TA-DIB-Fe) copolymer. The polymer fragments can be remolded into different shapes under given pressure at room temperature for 24 h (Fig. 2.12A). The recycled copolymers by this method showed only minor fatigue in mechanical moduli and breaking elongation (Fig. 2.12B), suggesting the great potential of this polymer to be applied in reusable plastics and materials.

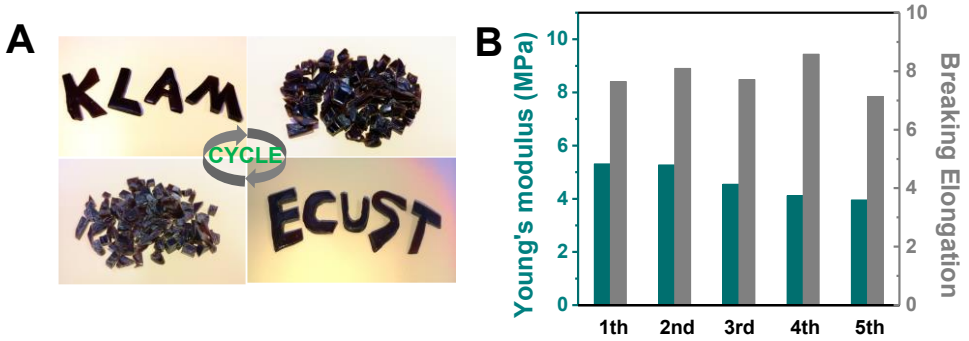

Figure 2.12 (A) Photographs of the reprocessed polymer with different shapes. (B) Mechanical properties of the recycled polymers during five cycles.

2.3 Conclusions

In summary, we have demonstrated a toughening strategy for a low-modulus supramolecular network by introducing high-density iron(III)-carboxylate complexes to form secondary ionic clusters. The toughened dry network exhibited remarkably increased mechanical moduli (63 times higher than the original network), high stretchability, self-healing ability at room temperature, water-insensitivity, and reversible processability under mild conditions. This study also supports a successful example in the exploration toward the fundamental question whether high-density metal-ligand combinations could simultaneously facilitate the mechanical properties and self-healing performance of dry polymers. We envision that this low-cost, natural-product-based and high-performance material might play a prominent role in many practical applications, including wearable devices, protective coatings and biomedical materials.

2.4 Acknowledgements and Contributions

This work was supported by National Natural Science Foundation of China (grants 21788102, 21790361, 21871084, 21672060, 21421004), Shanghai Municipal Science and Technology Major Project (Grant No.2018SHZDZX03), the Fundamental Research Funds for the Central Universities, the Programme of Introducing Talents of Discipline to Universities (grant B16017), and the Shanghai Science and Technology Committee (grant 17520750100). Ben L. Feringa acknowledges financial support of the Netherlands Ministry of Education, Culture

and Science (Gravitation program 024.601035). We appreciate Dr. Na Li (BL19U2 beamline of Shanghai Synchrotron Radiation Facility) for her kind help in synchrotron radiation SAXS test. Miss Qi Wei and Prof. Zhijun Ning (Shanghai Tech University) for their kind help in GIWAXS experiments. We also thank the Research Center of Analysis and Test of East China University of Science and Technology for the help on the material characterization.

Y.D. devised the project, synthesized all polymers, conducted all experiments on mechanical property and self-healing ability and wrote the manuscript. Q.Z devised, guided the project and contributed to the manuscript. B.L.F, H.T. and D.H.Q guided the project and contributed to the manuscript.

2.5 Experimental Section

2.5.1 Materials

All the reagents were purchased from Adamas®beta, TCI and Aldrich. The key feedstock (±)-α-thioctic acid (TA) was used as received from Adamas®beta with a Reagent Grade (99%). Diisopropenylbenzene (DIB) was used as received from TCI.

2.5.2 Preparation of poly(TA-DIB-Fe)

TA powder (25 g) was added to a flask and then heated in an oil bath (150°C) to form a yellow transparent low-viscosity molten TA liquid. DIB (5 g, 20 wt %) was added into the liquid by injection and further stirred at 150°C for 5 min. Then a given amount of $FeCl_3 \cdot 6H_2O$ [Iron(III)-to-TA molar ratio of 1/50, 1/100, 1/500, 1/1000 and 1/18000, respectively] was dissolved in a minimal amount of acetone, which was added to the liquid mixture under vigorous stirring. The liquid mixture was then poured into the desired mould, and a dark brown solid copolymer was obtained after cooling down to room temperature.

2.5.3 Methods for mechanical test

All stress-strain curves were obtained from a HY-0580 tension machine (HENGYI Company). The cylindrical shaped tested samples (height, 15 mm; diameter, 4.72 mm) were obtained by moulding in plastic injection syringes. The initial length was controlled between 8 ~ 10 mm. Unless otherwise noted, the tensile stress was

measured at a constant speed of 50 mm min^{-1}. The data were recorded in real time by a connected computer.

The strain rate indeed makes considerable differences on the tensile stress curves, and hence we have labeled all the strain rates of the corresponding tensile strain curves. Widely used are 20 mm/min or lower rates as the strain rates for rubber material test as reported in many papers:

Bao, et al. *Nat. Chem.* 2016, 8, 618 (used strain rate:10 mm/min);
Vlassak, et al. *Adv. Mater.* 2016, 28, 4678 (used strain rate: 15 mm/min);
Panzer, et al. *Chem. Mater.* 2019, 31, 2913 (used strain rate: 6 mm/min);
Yu, et al. *Nat. Comm.* 2018, 9, 2786 (used strain rate: 10 mm/min);
Wang, et al. *Angew. Chem. Int. Ed.* 2018, 57, 1361 (used strain rate: 5 mm/min);
Cheng, et al. *Angew. Chem. Int. Ed.* 2020, 59, 395 (used strain rate: 10 mm/min);

Hence, 20 mm/min is an applicable strain rate for rubber materials. The “flowing” behavior exists in polymer stretching, which is the intrinsic highly dynamic nature of the network, that is the fast exchange of noncovalent bond and polymer chain sliding process. This is also the reason of the stretchability of this material.

2.5.4 Methods for healing test

The copolymer cylinder (height, 15 mm; diameter, 4.5 mm) was cut into two identical pieces by a knife, and the interfaces were contacted immediately followed by slight extrusion for interface contact. The self-healing process was performed at room temperature (15 ~ 20°C). The stress-strain curves of the healed samples were obtained from the mechanical test described above.

2.6 Supplemental figures

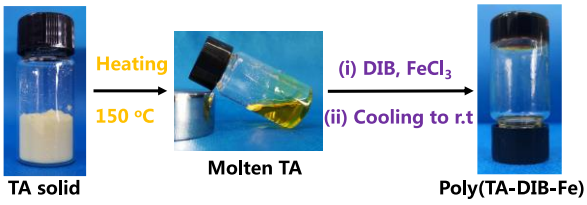

Figure S1. Photographs of the synthetic process of poly(TA-DIB-Fe) copolymer by a facile one-pot method.

A

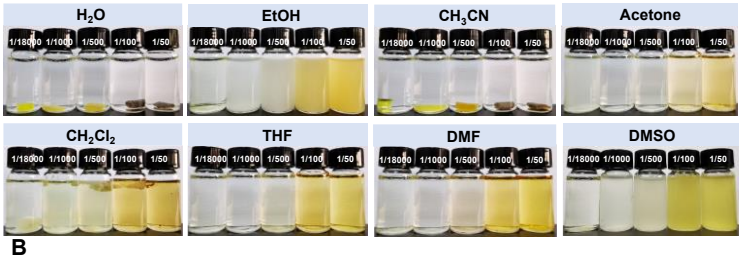

B

Fe/TA	H_2O	EtOH	CH_3CN	Acetone	CH_2Cl_2	THF	DMF	DMSO
1/18000	X	Partial	X	√	Partial	√	√	Partial
1/1000	X	Partial	X	√	Partial	√	√	Partial
1/500	X	Partial	X	√	Partial	√	√	Partial
1/100	X	Partial	X	Partial	Partial	√	Partial	Partial
1/50	X	Partial	X	Partial	Partial	√	Partial	Partial

Figure S2. Solubility test of the resulting poly(TA-DIB-Fe) copolymer with different Fe/TA molar ratios. (A) Photographs of the polymer samples soaked in different solvents for 24 h; (B) Tables of the relationships between solvent solubility and Fe/TA molar ratio. ("✓" means totally soluble; "Partial" means partially soluble; "X" means insoluble).

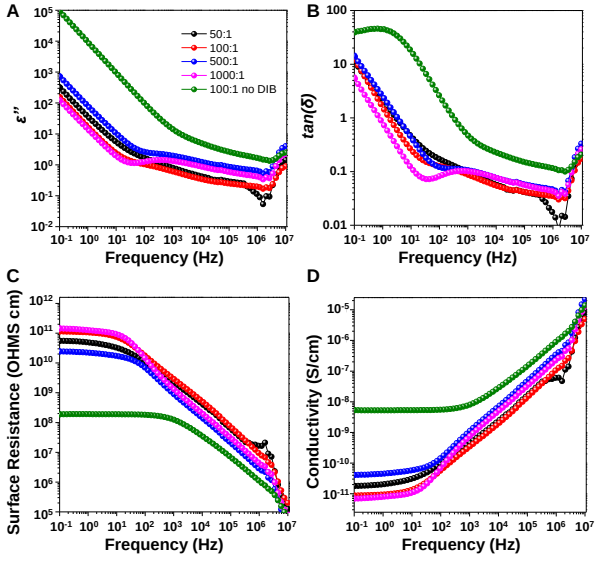

Figure S3. Broadband dielectric spectroscopy of poly(TA-DIB-Fe) copolymers with varied iron(III)-to-TA molar ratio. (A) dielectric constant (*ε''*), (B) dielectric loss (*tan(δ)*), (C) surface resistance, and (D) Conductivity versus frequency of the copolymer. The

iron(III)-to-TA molar ratios are 1/50, 1/100, 1/500, and 1/1000. A reference sample was also tested with the "softened" Poly(TA-Fe) polymer with iron(III)-to-TA molar ratio of 1/100 but without DIB.

Table S1. Summary of mechanical properties of poly(TA-DIB-Fe) copolymers with different ratio (measured at a stretching speed of 50 mm min^{-1})

	Maximal strength [MPa]	Strain at break [%]	Breaking strength [MPa]	Young's modulus [MPa]
1/50	1.87	599	1.87	7.78 ± 0.46
1/100	1.30	982	1.28	5.10 ± 0.12
1/500	0.38	2520	0.33	1.06 ± 0.03
1/1000	0.16	>8000	--	0.83 ± 0.04
1/18000	0.05	>8000	--	0.086 ± 0.01

Figure S4. The recovered poly(TA-DIB-Fe) copolymer [Iron(III)-to-TA molar ratio of 1/100] after stressed.

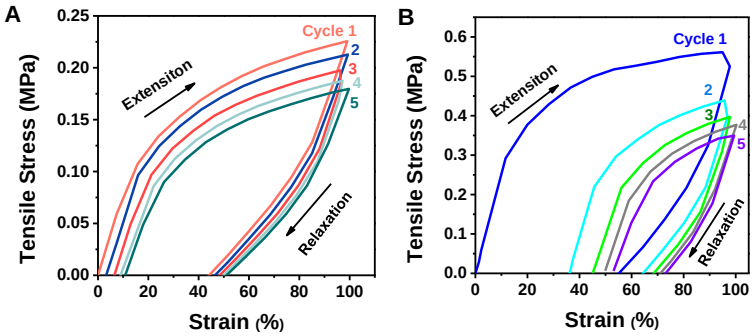

Figure S5. Five successive loading-unloading cycles of copolymers. (A) Poly(TA-DIB-Fe) copolymer [Iron(III)-to-TA molar ratio of 1/500] with 5 min rest intervals; (B) Poly(TA-DIB-Fe) copolymer [Iron(III)-to-TA molar ratio of 1/100] with 10 s rest intervals.

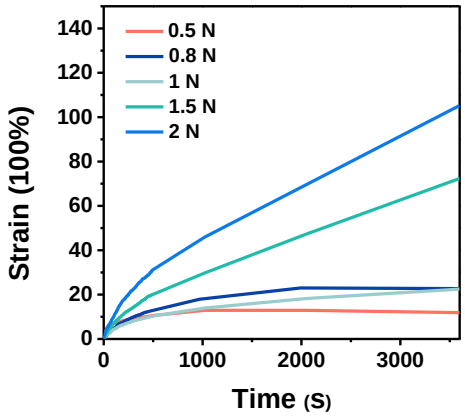

Figure S6. Creep experiments of the poly(TA-DIB-Fe) copolymer [Iron(III)-to-TA molar ratio of 1/100].

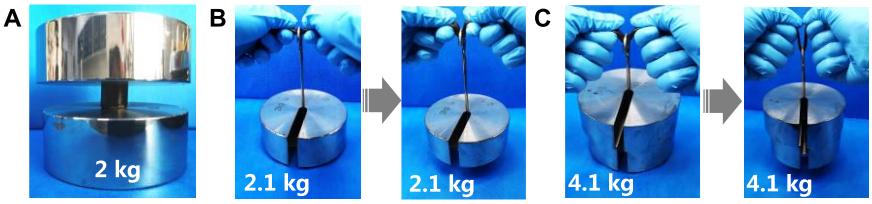

Figure S7. The visual mechanical characterization. The photographs of load bearing test of (A) cylindrical poly(TA-DIB-Fe) copolymer and (B), (C) poly(TA-DIB-Fe) copolymer film with a thickness of 2 mm [Iron(III)-to-TA molar ratio of 1/100].

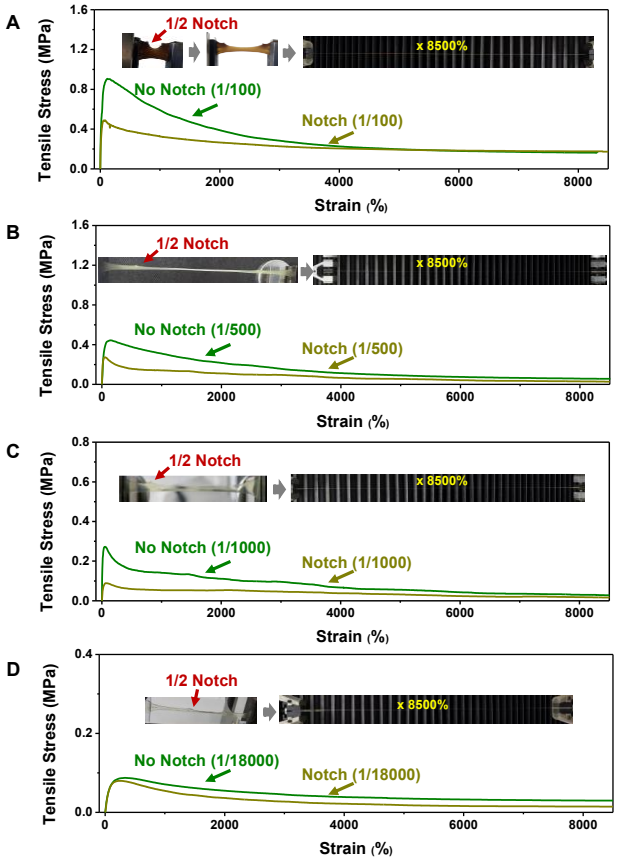

Figure S8. Stress-strain curves of the 1/2 notch copolymer samples with different iron(III)-to-TA molar ratios. The stretching speed is 20 mm min^{-1}. (A) 1/100; (B) 1/500; (C) 1/1000; (D) 1/18000.

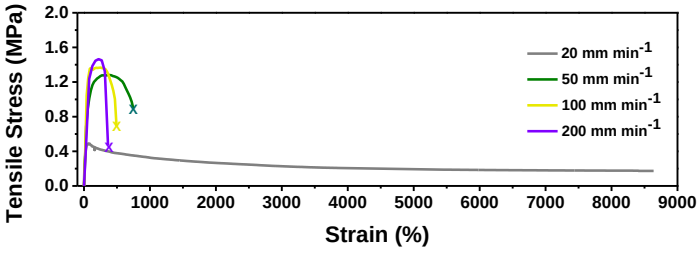

Figure S9. Stress-strain curves under different stretching speed of the copolymer sample with a pre-damaged 1/2 notch. The iron(III)-to-TA molar ratio was 1/100.

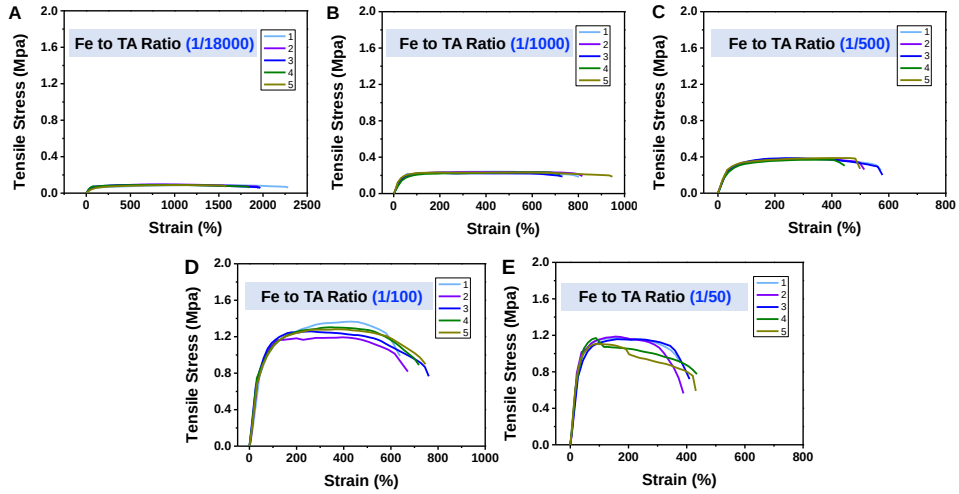

Figure S10. Reproduced stress-strain curves of the 1/2 notch copolymer samples with different iron(III)-to-TA molar ratios. The stretching speed is 50 mm min^{-1}. Five parallel tests were performed for reproducibility. The tensile stress of the notched samples has been corrected by the real area after notching.

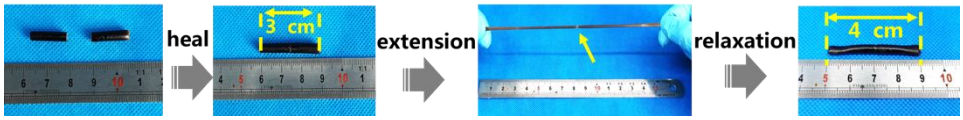

Figure S11. Two cutting pieces of poly(TA-DIB-Fe) copolymer [iron(III)-to-TA molar ratio of 1/100] were touched to heal at room temperature for 10 min, and the healed sample (3 cm) can be stretched to over 15 cm and recover to 4 cm after 2 min.

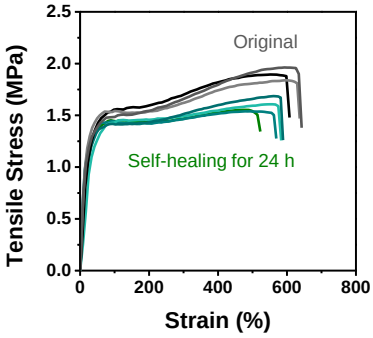

Figure S12. Stress-strain curve of the original and healed copolymer with an iron(III)-to-TA molar ratio of 1/50. The self-healing experiments are performed at room temperature for 24 h. Parallel experiments are shown for reproducibility.

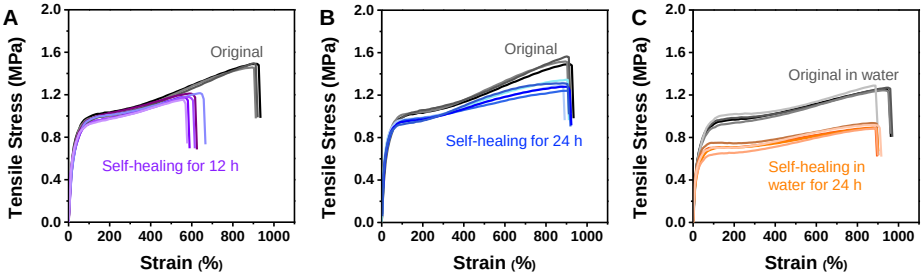

Figure S13. Stress-strain curves of the original and healed samples of poly(TA-DIB-Fe) copolymer. (A) Self-healing for 12 h at room temperature in air; (B) Self-healing for 24 h at room temperature in air; (C) Self-healing for 24 h at room temperature under water; The iron(III)-to-TA molar ratio was 1/100. Tensile speed is 50 mm min^{-1}. Parallel self-healing experiments are performed 5 times for showing reproducibility.

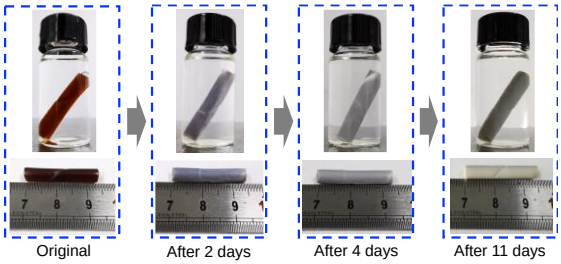

Figure S14. Photographs of the poly(TA-DIB-Fe) copolymer soaked in water for several days. The clear solution suggested no dissolution, and the unchanged length of sample indicated no visible swelling process. The turbidity of the sample became increased after long-term soaking, which might be attributed to the presence of phase separation in the network by the absorbed water and hydrophobic network.

2.7 References

1. a) P. Cordier, F. Tournilhac, C. Soulié-Ziakovic, L. Leibler, *Nature*, **2008**, *451*, 977; b) B. Ghosh, M. W. Urban, *Science,* **2009**, *323*, 1458; c) M. Burnworth, L. Tang, J. R. Kumpfer, A. J. Duncan, F. L. Beyer, G. L. Fiore, S. J. Rowan, C. Weder, *Nature*, **2011**, *472*, 334; d) E. J. Markvicka, M. D. Bartlett, X. Huang, C. Majidi, *Nat. Mater.* **2018**, *17*, 618; e) M. W. Urban, D. Davydovich, Y. Yang, T. Demir, Y. Zhang, L. Casabianca, *Science*, **2018**, *362*, 220; f) T. Sekitani, Y. Noguchi, K. Hata, T. Fukushima, T. Aida, T. Someya, *Science*, **2018**, *321*, 1468; g) D. Son, J. Kang, O. Vardoulis, Y. Kim, N. Matsuhisa, J. Y. Oh, J. W. F. To, J. Mun, T. Katsumata, Y. Liu, A. F. McGuire, M. Krason, F. Molina-Lopez, J. Ham, U. Kraft, Y. Lee, Y. Yun, J. B. H. Tok, Z. Bao, *Nat. Nanotech.* **2018**, *13*, 1057; h) R. P. Wool, *Soft*

Matter, **2008**, *4*, 400.

2. a) Y. Chen, A. M. Kushner, G. A. Williams, Z. Guan, *Nat. Chem.* **2012**, *4*, 467; b) Y. Song, Y. Liu, T. Qi, G. H. Li, *Angew. Chem. Int. Ed.* **2018**, *57*, 13838; c) M. Liu, P. Liu, H. Lu, Z. Xu, X. Yao, *Angew. Chem. Int. Ed.* **2018**, *57*, 11242; d) X. Yan, Z. Liu, Q. Zhang, J. Lopez, H. Wang, H.-C. Wu, S. Niu, H. Yan, S. Wang, T. Lei, J. Li, D. Qi, P. Huang, J. Huang, Y. Zhang, Y. Wang, G. Li, J. B.-H. Tok, X. Chen, Z. Bao, *J. Am. Chem. Soc.* **2018**, *140*, 5280; e) J. Kang, D. Son, G.-J. N. Wang, Y. Liu, J. Lopez, Y. Kim, J. Y. Oh, T. Katsumata, J. Mun, Y. Lee, L. Jin, J. B.-H. Tok, Z. Bao, *Adv. Mater.* **2018**, *30*, e1706846l; f) R. Tamate, K. Hashimoto, T. Horii, M. Hirasawa, X. Li, M. Shibayama, M. Watanabe, *Adv. Mater.* **2018**, *30*, e1802792; g) D. W. Balkenende, C. A. Monnier, G. L. Fiore, C. Weder, *Nat. Comm.* **2016**, *7*, 10995. h) D. Montarnal, F. Tournilhac, M. Hidalgo, J. L. Couturier, L. Leibler, *J. Am. Chem. Soc.* **2009**, *131*, 7966.
3. a) J. Liu, C. S. Y. Tan, Z. Yu, N. Li, C. Abell, O. A. Scherman, *Adv. Mater.* **2017**, *29*, e1605325; b) Z. Wang, Y. Ren, Y. Zhu, L. Hao, Y. Chen, G. An, H. Wu, X. Shi, C. Mao, *Angew. Chem. Int. Ed.* **2018**, *57*, 9008; c) Q. Zhang, R. J. Xing, W. Z. Wang, Y. X. Deng, D. H. Qu, H. Tian, *iScience*, **2019**, *19*, 14; d) M. Nakahata, S. Mori, Y. Takashima, H. Yamaguchi, A. Harada, *Chem*, **2016**, *1*, 766; e) C. Lu, M. Zhang, D. Tang, X. Yan, Z. Zhang, Z. Zhou, B. Song, H. Wang, X. Li, S. Yin, H. Sepehrpour, P. J. Stang, *J. Am. Chem. Soc.* **2018**, *140*, 7674.
4. a) D. Mozhdehi, S. Ayala, O. R. Cromwell, Z. Guan, *J. Am. Chem. Soc.* **2014**, *136*, 16128; b) C.-H. Li, C. Wang, C. Keplinger, J.-L. Zuo, L. Jin, Y. Sun, P. Zheng, Y. Cao, F. Lissel, C. Linder, X.-Z. You, Z. Bao, *Nat. Chem.* **2016**, *8*, 618; c) J. C. Lai, L. Li, D. P. Wang, M. H. Zhang, S. R. Mo, X. Wang, K. Y. Zeng, C. H. Li, Q. Jiang, X. Z. You, J. L. Zuo, *Nat. Comm.* **2018**, *9*, 2725; d) Q. Zhang, S. Niu, L. Wang, J. Lopez, S. Chen, Y. Cai, R. Du, Y. Liu, J. C. Lai, L. Liu, C. H. Li, X. Yan, C. Liu, J. B. H. Tok. X. Jia, Z. Bao, *Adv. Mater.* **2018**, *30*, e1801435; e) E. Khare, N. Holten-Andersen, M. J. Buehler, *Nat. Rev. Mat.* **2021**, *6*, 421-436.
5. a) P. Guo, H. Zhang, X. Liu, J. Sun, *ACS Appl. Mater. Interfaces*, **2018**, *10*, 2105; b) Z. Lei, P. Wu, *Nat. Comm.* **2018**, *9*, 1134; c) Z. Lei, P. Wu, *Nat. Comm.* **2019**, *10*, 3429; d) X. Fang, J. Sun, *ACS Macro Lett.* **2019**, *8*, 500; e) A. J. D'Angelo, M. J. Panzer, *Chem. Mater.* **2019**, *31*, 2913; f) S. Stein, A. Mordvinkin, B. Voit, H. Komber, K. Saalwächter, F. Böhme, *Polym. Chem.* **2020**, DOI: 10.1039/C9PY01630A; g) S. K. Kalista, T. C. Ward, *J. R. Soc. Interface*, **2007**, *4*, 405.
6. a) X. H. Lu, Z. Guan, *J. Am. Chem. Soc.* **2012**, *134*, 14226; b) S. Ji, W. Cao, Y. Yu, H. Xu, *Adv. Mater.* **2015**, *27*, 7740; c) J. A. Neal, D. Mozhdehi, Z. Guan, *J. Am. Chem. Soc.* **2015**, *137*, 4846; d) H. Qin, T. Zhang, H. N. Li, H. P. Cong, M. Antonietti, S. H. Yu, *Chem*, **2017**, *3*, 691; e) C. Bao, Y. J. Jiang, H. Zhang, X. Lu, J. Sun, *Adv. Funct. Mater.* **2018**, *28*, 1800560; f) S. J. Rowan, S. J. Cantrill, G. R. L. Cousins, J. K. M. Sanders, J. F. Stoddart, *Angew. Chem. Int. Ed.* **2002**, *41*, 898-952; g) J. -M. Lehn,

Chem. Soc. Rev., **2007**, *36*, 151-160.

7. Y. Cao, H. Wu, S. I. Allec, B. M. Wong, D. S. Nguyen, C. Wang, *Adv. Mater.* **2018**, *30*, e1804602.
8. Q. Zhang, C. Y. Shi, D. H. Qu, Y. T. Long, B. L. Feringa, H. Tian, *Sci. Adv.* **2018**, *4*, eaat8192.
9. C. J. Carrano, H. Drechsel, D. Kaiser, G. Jung, B. Matzanke, G. Winkelmann, N. Rochel, A. M. Albrecht-Gary, *Inorg. Chem.* **1996**, *35*, 6429.
10. R. L. Rardin, P. Poganiuch, A. Bino, D. P. Goldberg, W. B. Tolman, S. Liu, S. J. Lippard, *J. Am. Chem. Soc.* **1992**, *114*, 5240.
11. E. Filippidi, T. R. Cristiani, C. D. Eisenbach, J. H. Waite, J. N. Israelachvili, B. K. Ahn, M. T. Valentine, *Science*, **2017**, *358*, 502.
12. a) Q. Zhang, Y. X. Deng, H. Luo, C. Y. Shi, G. M. Geise, B. L. Feringa, H. Tian, D. H. Qu, *J. Am. Chem. Soc.* **2019**, *141*, 12804; b) Q. Zhang, T. Li, A. Duan, S. Dong, W. Zhao, P. J. Stang, *J. Am. Chem. Soc.* **2019**, *141*, 8058.
13. F. Kremer, A. Schönhals, Eds., Broadband Dielectric Spectroscopy (Springer, 2002).
14. S. Dong, J. Leng, Y. Feng, M. Liu, C. J. Stackhouse, A. Schönhals, L. Chiappisi, L. Gao, W. Chen, J. Shang, L. Jin, Z. Qi, C. A. Schalley, *Sci. Adv.* **2017**, *3*, eaao0900.
15. M. Suckow, A. Mordvinkin, M. Roy, N. K. Singha, G. Heinrich, B. Voit, K. Saalwächter, F. Böhme, *Macromolecules,* **2018**, *51*, 468.
16. a) D. L. Taylor, M. in het Panhuis, *Adv. Mater.* **2016**, *28*, 9060; b) Z. Wei, J. H. Yang, J. Zhou, F. Xu, M. Zrínyi, P. H. Dussault, Y. Osada, Y. M. Chen, *Chem. Soc. Rev.* **2014**, *43*, 8114; c) D. Y. Wu, S. Meure, D. Solomon, *Prog. Polym. Sci.* **2008**, *33*, 479; d) C. E. Diesendruck, N. R. Sottos, J. S. Moore, S. R. White, *Angew. Chem. Int. Ed.* **2015**, *54*, 10428.
17. a) A. M. Kushner, J. D. Vossler, G. A. Williams, Z. Guan, *J. Am. Chem. Soc.* **2009**, *131*, 8766; b) P. F. Cao, B. Li, T. Hong, J. Townsend, Z. Qiang, K. Xing, K. D. Vogiatzis, Y. Wang, J. W. Mays, A. P. Sokolov, T. Saito, *Adv. Funct. Mater.* **2018**, *28*, e1800741; c) I. Jeon, J. Cui, W. R. K. Illeperuma, J. Aizenberg, J. J. Vlassak, *Adv. Mater.* **2016**, *28*, 4678; d) Y. Wang, X. Liu, S. Li, T. Li, Y. Song, Z. Li, W. Zhang, J. Sun, *ACS Appl. Mater. Interfaces*, **2017**, *9*, 29120; e) J. Wu, L. H. Cai, D. A. Weitz, *Adv. Mater.* **2017**, *29*, e1702616; f) M. A. Darabi, A. Khosrozadeh, R. Mbeleck, Y. Liu, Q. Chang, J. Jiang, J. Cai, Q. Wang, G. Luo, M. Xing, *Adv. Mater.* **2017**, *29*, e1700533. g) S. Wang, M. W. Urban, *Nat. Rev. Mat.* **2020**, *5*, 562-583.
18. a) Z. Zou, C. Zhu, Y. Li, X. Lei, W. Zhang, J. Xiao, *Sci. Adv.* **2018**, *4*, eaaq0508; b) G. Chang, L. Yang, J. Yang, M. P. Stoykovich, X. Deng, J. Cui, D. Wang, *Adv. Mater.* **2018**, *30*, 1704234; c) S. Westhues, J. Idel, J. Klankermayer, *Sci. Adv.* **2018**, *4*, eaat9669; d) E. M. Lloyd, H. L. Hernandez, A. M. Feinberg, M. Yourdkhani, E. K. Zen, E. B. Mejia, N. R. Sottos, J. S. Moore, S. R. White, *Chem. Mater.* **2019**, *31*, 398; e) F. Lossada, D. Jiao, X. Yao, A. Walther, *ACS Macro Lett.* **2020**, *9*, 70.